Reorganization Parameters of Electronic Transitions in Electronically Delocalized Systems. 2. Optical Spectra

Dmitry V. Matyushov*,† and Gregory A. Voth*

Department of Chemistry and Henry Eyring Center for Theoretical Chemistry, University of Utah, 315 South 1400 East, Salt Lake City, Utah 84112

Received: November 2, 1999; In Final Form: March 3, 2000

This is a modification of the condensed-phase band shape analysis of optical spectra to treat electronically delocalized systems. It incorporates the dependence of the optical observables on the optical transition dipole. Absorption and emission band shapes are calculated on the basis of adiabatic free energy surfaces defined as the functions of the reorganization parameters invariant to electronic delocalization and the parameter of electronic delocalization. The latter is given through the ratio of the transition and differential chromophore dipoles. The linear response relations commonly used to connect optical observables to reorganization parameters of electron transfer reactions break down for electronically delocalized systems. The optical Stokes shift depends strongly on the delocalization parameter deviating downward from twice the adiabatic reorganization energy with electronic delocalization. The Stokes shift is a rising function of solvent polarity for localized systems. An inverted solvent dependence develops for delocalized complexes: the Stokes shift decreases with solvent polarity. The spectrum of permissible solvent fluctuations is limited from the low-energy side by the adiabatic splitting of the free energy terms inducing narrowing of the emission optical bands compared to the absorption bands.

1. Introduction

Classical theories of optical band shapes in condensed phases consider electronic transitions between distinct electronic states, each characterized by a distribution of the electronic density.[1] The electronic density changes instantaneously, on the nuclear time scale, with electronic transition (the Franck−Condon principle).[2] The interaction of the differential charge distribution in the two states with the nuclear modes equilibrated to the solute in the initial electronic state generates the nuclear component of the steady-state spectral band shape. Because nuclear configurations are statistically distributed, spectral lines get inhomogeneously broadened.[3]

This basic picture of optical band shapes in condensed phases involves the important assumption that the electronic charge distributions characteristic of the ground and excited states do not change with fluctuations of the solvent field.[1] This model is isomorphic to the diabatic (localized) description of electron transfer (ET) reactions embodied in the Marcus−Hush theory of ET.[4] It suggests that the transferred electron is fully localized in one state until it hops to another state when the resonance of the electronic levels is reached through the fluctuations of the nuclear coordinates coupled to the electronic states (Robin−Day class II[5]). Not surprisingly, the isomorphism of physical models is projected into isomorphism of theoretical descriptions of thermally activated ET reactions and optical transitions.[6]

Coupling of the solute electronic states to the solvent is fundamentally based on electrostatic interactions between the solute electronic density and charges localized on the solvent molecules. Because this interaction is long-ranged, many solvent molecules are involved in the solvent response. The solvent response can be characterized by a number of Gaussian collective modes coupled to the solute,[7] producing an essentially Gaussian distribution of the solute electronic density of states. The solvent is then said to be linearly responding.

Several very general relations between optical observables can be obtained for linearly responding (Gaussian) solvents interacting with a fixed charge distribution of the solute. The energetic intensity of the solvent nuclear fluctuations coupled to the solute can be characterized by the single parameter, the solvent reorganization energy, λ_s^d.[4] Here, the superscript "d" refers to the diabatic representation implying that the charge is fully localized in each electronic state. Several spectroscopic observables can be related to λ_s^d. The solvent-induced component of the Stokes shift $h\Delta\nu_s^{st}$ generates the reorganization energy

$$\lambda_s^{st} = h\Delta\nu_s^{st}/2, \quad \Delta\nu_s^{st} + \Delta\nu_v^{st} = \nu_{abs} - \nu_{em} \tag{1}$$

The solvent-induced absorption, σ_{abs}, and emission, σ_{em}, spectral widths also yield the solvent reorganization energies

$$\lambda_{abs}^{w} = \beta\sigma_{abs}^2/2, \quad \lambda_{em}^{w} = \beta\sigma_{em}^2/2 \tag{2}$$

where $\beta = 1/k_BT$ and, in eq 1, $\Delta\nu_v^{st}$ is the solute vibronic component of the Stokes shift.[8]

When each electronic state is characterized by a certain charge distribution unchanged with solvent configurations (diabatic or localized representation), the reorganization energies from optical spectroscopy are equal to the diabatic reorganization energy λ_s^d entering the activation barrier of ET reactions[6]

$$\lambda_s^d = \lambda_s^{st} \tag{3}$$

and

† Present address: Department of Chemistry and Biochemistry, Arizona State University, P.O. Box 871604, Tempe, AZ 85287-1604.

10.1021/jp9938866 CCC: $19.00
Published on Web 06/17/2000

$$\lambda_s^d = \lambda_{abs}^w = \lambda_{em}^w \tag{4}$$

In addition, the free energy gap between the initial and final electronic states is the mean of the optical transition energies

$$\Delta F_0^d = h\nu_m = h(\nu_{abs} + \nu_{em})/2 \tag{5}$$

Equations 3−5 are exact for any fixed charge distribution of the solute in a linearly responding solvent. Several attempts have been undertaken to challenge the representation of the solvent response by a collection of Gaussian modes.[9] Although some deviations from the linear behavior do exist, they are usually relatively small. The basic result of these studies is that the action of a dense solvent on a fixed charge distribution of a solute is indeed well represented by the linear solvent response. The next question that arises is what would be the effect of relaxing the assumption of a fixed charge distribution of the solute. Addressing this problem is the motivation of the present study. We approach the question of what happens when the electronic density is allowed to flow between the initial and final states, i.e., the effect of electronic delocalization.

Delocalization of the electronic density between the initial and final states alters the solute electric field, thus modifying the solute−solvent coupling and the line shift. But the strongest effect of delocalization is expected to occur on the inhomogeneous broadening and the observed optical width. This is because, in an electronically delocalized solute, the charge distribution changes instantaneously with solvent configuration, so that each configuration "sees" a different charge distribution.[10] This self-consistent action results in essentially nonlinear features of the solvent effect (e.g., the self-energy of the solute electronic subsystem changes with solvent fluctuations).[11] Therefore, despite the fact that solvent fluctuations are still Gaussian, solute electronic self-consistency destroys the linear response regime and relations 3−5 break down. The present paper quantifies this effect.

In the preceding paper,[12] the CT adiabatic free energy surfaces, $F_\pm(X)$, along the reaction coordinate X coupling a two-state solute to the nuclear solvent polarization of the solvent have been derived. The lower, $F_-(X)$, and upper, $F_+(X)$, adiabatic surfaces are functions of the reorganization parameters that are invariant in respect to the unitary transformations of the solute wave function basis (and thus invariant to electronic delocalization) and the delocalization parameter Δe. The latter is defined through the vacuum transition, m_{12}, and differential, Δm_{12}, *adiabatic* solute dipoles as

$$\Delta e = \left[1 + \frac{4m_{12}^2}{\Delta m_{12}^2}\right]^{-1/2} \tag{6}$$

The dependence on Δe incorporates the dependence of $F_\pm(X)$, and with that of optical observables, on the transition dipole.

Optical absorption and emission result from Franck−Condon transitions between the lower and upper adiabatic ET surfaces. They are, therefore, used to construct the absorption and emission band profiles (section 2). With inclusion of the intramolecular vibrational excitations, this provides an extension of the classical band shape analysis of optical spectra[13,14] to electronically delocalized systems (section 2.3). In section 3, the effect of electronic delocalization on optical spectra in the normal (section 3.1) and inverted (section 3.2) regions of ET are analyzed. It turns out that eqs 3−5 hold only in a very narrow range of Δe values close to unity. Especially the Stokes shift is a strongly decaying function of Δe. It depends on solvent polarity as the reorganization energy for Δe close to unity and then reverses its solvent dependence with decreasing delocalization parameter. Also the widths of the absorption and emission lines differ substantially when $\Delta e < 1$. These results are discussed and compared to traditional theories in section 4. Finally, section 5 concludes.

2. Absorption and Emission Intensities

2.1. Free Energy Surfaces. In the preceding paper,[12] we have considered a two-state solute which electric field interacts with the polarization of the solvent P. The system Hamiltonian is

$$H = H_B[P] + \sum_{i=1,2} (E_i - E_i \cdot P) a_i^+ a_i - E_{12} \cdot P (a_1^+ a_2 + a_2^+ a_1) \tag{7}$$

where $H_B[P]$ is the Hamiltonian of a linearly responding solvent and a_i^+ and a_i are the operators of creation and annihilation in the adiabatic vacuum states Ψ_i with the energies E_i, $i = 1, 2$. The energies E_i refer to the Born−Oppenheimer electronic terms in a vacuum at equilibrium configuration of the intramolecular nuclear modes of the solute. The operator of the solute electric field $\hat{E}$ has the diagonal $E_{ii} = E_i$ and off-diagonal E_{12} matrix elements. Throughout below we will consider a dipolar solute for which $E_{ij} = \mathbf{m}_{ij} \cdot \mathbf{T}$, where $\mathbf{T}$ is the dipolar tensor and $\mathbf{m}_{ij} = \langle \Psi_i | \hat{\mathbf{m}} | \Psi_j \rangle$.

The CT free energy along the reaction coordinate $X = \Delta E \cdot P_n$ ($\Delta E = E_2 - E_1$, P_n is the nuclear component of the solvent polarization) can be separated into the lower and upper CT surfaces which are the eigenvalues of the two-state matrix[12]

$$\begin{pmatrix} V_1(X) + X/2 & \alpha_{12}(\Delta e \Delta F_s^I - X) \\ \alpha_{12}(\Delta e \Delta F_s^I - X) & V_2(X) - X/2 \end{pmatrix} \tag{8}$$

with $\alpha_{12} = m_{12}/\Delta m_{12}$ and

$$V_i(X) = F_{0i}^{ad} + \frac{X^2}{4\Delta e^2 \lambda_s^I} + \frac{\Delta e^2 \lambda_s^I}{4} \tag{9}$$

Here, ΔF_s^I and λ_s^I are the solvent-induced component of the free energy gap and the solvent reorganization energy, respectively. Both are invariant to the unitary transformations of the solute basis thus keeping the same values in the adiabatic and diabatic representations. Diagonalization of eq 8 results in the lower "−" and upper "+" CT free energy surfaces

$$F_\pm(X) = \frac{X^2}{4\Delta e^2 \lambda_s^I} \pm \frac{1}{2}\Delta E(X) + C \tag{10}$$

with

$$\Delta E(X) = [\Delta E^2 + 2\Delta E(\Delta e \Delta F_s^I - X) + (\Delta F_s^I - X/\Delta e)^2]^{1/2} \tag{11}$$

and

$$C = \frac{F_{01}^{ad} + F_{02}^{ad}}{2} + \frac{\Delta e^2 \lambda_s^I}{4} \tag{12}$$

In eq 9, F_{0i}^{ad} is the adiabatic, equilibrium free energy in the ith state so that the adiabatic free energy gap is $\Delta F_0^{ad} = F_{02}^{ad} - F_{01}^{ad} = \Delta E + \Delta e \Delta F_s^I$. Here, $\Delta E = E_2 - E_1$ refers to the 0−0 vacuum transition energy that can be determined through the

vacuum absorption $h\nu_{abs}^{(0)} = \Delta E + \lambda_v$ and emission $h\nu_{em}^{(0)} = \Delta E - \lambda_v$ energies as $\Delta E = h(\nu_{abs}^{(0)} + \nu_{em}^{(0)})/2$. The vacuum adiabatic gap ΔE is connected to the diabatic gap ΔI_{ab} (the difference in a vacuum electronic energies of noninteracting donor and acceptor units) and the ET matrix element H_{ab} by the relations

$$\Delta E = [\Delta I_{ab}^2 + 4|H_{ab}|^2]^{1/2} \tag{13}$$

and becomes $2|H_{ab}|$ for self-exchange transitions with $\Delta I_{ab} = 0$. The gap ΔF_0^{ad} defines the point of intersection of the diagonal matrix element in the adiabatic two-state matrix in eq 8. This point does not, however, coincide with the transition state due to the X dependence of the off-diagonal components of the Hamiltonian. The true free energy gap ΔF_0 defined as the difference between the free energies at the surface minima then differs from ΔF_0^{ad} and is in fact a discontinuous function of ΔF_0^{ad} when switching between the normal and inverted CT regions.[12]

The optical transitions proceed between the adiabatic free energy surfaces $F_-(X)$ and $F_+(X)$ that are the eigenvalues of the two-state matrix in eq 8. Correspondingly, the electronic states involved in the transitions are those diagonalizing the same matrix. These wave functions $\tilde{\Psi}_1(X)$ and $\tilde{\Psi}_2(X)$ depend on the solvent configuration through the reaction coordinate X. The extinction coefficient of absorption (cm^{-1} M^{-1}) then reads[2,12]

$$\frac{\epsilon(\nu)}{\nu} = A\frac{f^2(n_D)}{n_D} I_-(\nu) \tag{14}$$

where

$$A = \frac{8\pi^3 N_A}{3000\ln(10)c} \tag{15}$$

and for a reaction coordinate X treated in the classical limit

$$I_\pm(\nu) = \langle|\tilde{m}_{12}(X)|^2\delta(\Delta E(X) - h\nu)\rangle_\pm \tag{16}$$

In eq 15, N_A is the Avogadro number and c is the velocity of light in a vacuum.

The spectral functions $I_\pm(\nu)$ involve the average over the equilibrium distribution of reaction coordinates

$$\langle ...\rangle_\pm = (Q_\pm)^{-1}\int_{-\infty}^{\infty} ... e^{-\beta F\pm(X)} dX \tag{17}$$

with

$$Q_\pm = \int_{-\infty}^{\infty} dX e^{-\beta F\pm(X)} \tag{18}$$

The transition dipole in eq 16 is given by

$$|\tilde{m}_{12}(X)| = |\langle\tilde{\Psi}_1(X)|\hat{m}|\tilde{\Psi}_2(X)\rangle| = |\Delta m_{12}|\frac{\Delta E}{\Delta E(X)} \tag{19}$$

The function $f(n_D)$ of the refractive index n_D in eq 14 accounts for the deviation of the local field acting on a solute from the external electric field of the radiation. For spherical cavities, the dielectric theories predict[15]

$$f(n_D) = \frac{3n_D^2}{2n_D^2 + 1} \tag{20}$$

The emission rate $I_{em}(\nu)$ (number of photons per unit frequency) is related to the spectral function evaluated on the upper adiabatic surface

$$I_{em}(\nu) = \frac{64\pi^4\nu^3}{3c^3} n_D f^2(n_D) I_+(\nu) \tag{21}$$

In the next sections, we will be predominantly interested in the band shapes generated by the spectral functions $I_\pm(\nu)$. The spectral shifts and width are shown to be strongly affected by the extent of electronic delocalization characterized by the delocalization parameter Δe. The latter is determined by the adiabatic differential dipole (measured, e.g., by Stark spectroscopy[16]) and by the adiabatic transition dipole m_{12}. Both absorption and emission intensities can be employed to measure m_{12}. A relation of m_{12} to the integrated extinction coefficient is given in the preceding paper[12] in connection with the calculation of the ET matrix element. Here, a route through radiative rates is presented.

2.2. Radiative Rate. The vacuum transition dipole m_{12} is extracted from eqs 16 and 19 by noting that the integral $\int I_{em}(\nu)\nu^{-1}d\nu$ eliminates the dependence on X in the transition dipole $\tilde{m}_{12}(X)$. This yields for m_{12} (in debye)

$$m_{12} = 3.092 \times 10^8[\bar{\nu}_0\sqrt{n_D}f(n_D)]^{-1}[\int I_{em}(\nu)\nu^{-1}d\nu]^{1/2} \tag{22}$$

where $\bar{\nu}_0 = \Delta E/hc$ is the vacuum transition wavenumber (in cm^{-1}). When the emission spectrum is not available, the radiative rate

$$k_{rad} = \int I_{em}(\nu)d\nu = \Phi_{em}\tau_{em}^{-1} \tag{23}$$

can be used; Φ_{em} and τ_{em} are the quantum yield and emission lifetime. By defining the average frequency

$$\nu_{av} = \int I_{em}(\nu)d\nu / \int I_{em}(\nu)\nu^{-1}d\nu \tag{24}$$

one gets

$$m_{12} = 1.786 \times 10^3\left[\frac{k_{rad}}{\bar{\nu}_{av}\bar{\nu}_0^2 n_D f^2(n_D)}\right]^{1/2} \tag{25}$$

Equation 25 is not a very practical one as an accurate definition of the average wavenumber $\bar{\nu}_{av} = \nu_{av}/c$ demands knowledge of the emission spectrum for which eq 22 provides a direct route to the transition dipole. It can be used though in approximate calculations by assuming $\bar{\nu}_{av} = \bar{\nu}_{em}$.

Equation 25 is exact for a two-state solute, but differs from the traditionally used connection between the transition dipole and the emission intensity by the factor $\bar{\nu}_0/\bar{\nu}_{av}$.[17] The commonly used combination $m_{12}\bar{\nu}_0/\bar{\nu}_{av}$ can be associated with the condensed phase transition dipole in the two-state approximation.[18] The difference between the present and traditional formulations arises from the common assumption of independence of the transition dipole of the solvent configuration. The exact solution for a two-state solute makes the transition dipole between the adiabatic free energy surfaces be inversely proportional to the energy gap between them. This dependence is, however, eliminated when the emission intensity is integrated with the factor ν^{-1}. The necessity of this correction was noticed already by Gould et al.[19a] Their results were obtained by employing the first-order quantum mechanical perturbation theory (weak delocalization). The present formulation indicates that eqs 22 and 25 are valid for an arbitrary extent of electronic delocalization. Also note that m_{12} in eqs 22 and 25 is the *vacuum*

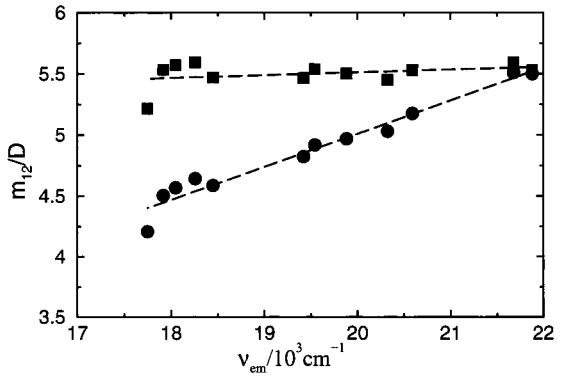

Figure 1. The transition dipole m_{12} according to eq 25 ($\bar{\nu}_{av} = \bar{\nu}_{em}$, circles) and $m_{12}\bar{\nu}_0/\bar{\nu}_{em}$ (squares) vs $\bar{\nu}_{em}$ for emission transitions in C153 in different solvents.[17b] The dashed lines are regressions with the slopes (squares) 0.02 and (circles) 0.27.

adiabatic transition dipole. Therefore, emission intensities measured in different solvents should generate invariant transition dipoles when treated according to eqs 22 and 25. A deviation from invariance can be used as an indication of the breakdown of the two-state approximation and existence of intensity borrowing from other excited states of the chromophore (the Murrell mechanism[19b,20]).

To illustrate the difference between the present and traditional formulations, Figure 1 shows the dependence of m_{12} (circles) and $m_{12}\bar{\nu}_0/\bar{\nu}_{av}$ (squares, $\bar{\nu}_0 = 25\,400$ cm^{-1})[21] on the emission frequency $\bar{\nu}_{em}$ for the coumarin-153 (C153) optical dye according to the data by Lewis and Maroncelli.[17b] Most noteworthy is a pronounced, approximately linear, dependence of m_{12} on the emission frequency. This is indicative of an emission borrowing to other excited states in contrast to the conclusion reached in ref 17b. Solvent independence of $m_{12}\bar{\nu}_0/\bar{\nu}_{av}$ points to of a significant mixing to other states.[19b,22]

2.3. Optical Band Shape. From eqs 16 and 19, the spectral functions $I_{\pm}(\nu)$ can be represented as follows

$$I_{\mp}(\nu) = \frac{1}{h}\left(\frac{\Delta m_{12}\Delta E}{h\nu}\right)^2 J_{abs,em}(\nu) \tag{26}$$

with the absorption (abs, "−") and emission (em, "+") intensities

$$J_{abs,em}(\nu) = h\langle\delta(h\nu - \Delta E(X))\rangle_{\mp} \tag{27}$$

obeying the normalization condition

$$\int_{-\infty}^{\infty} J_{abs,em}(\nu)\,d\nu = 1 \tag{28}$$

The integration over X can be performed directly in eq 27 with the result

$$J_{abs,em}(\nu) = h\sum_{k=1,2} |\Delta E'(X_k^*)Q_{\mp}|^{-1} \exp[-\beta F_{\mp}(X_k^*)] \tag{29}$$

Here

$$X_k^* = X_{min} \mp \Delta e\sqrt{(h\nu)^2 - \Delta E_{min}^2} \tag{30}$$

are the two solutions of the quadratic equation $\Delta E(X) = h\nu$ and

$$E_{min} = \Delta E\sqrt{1 - \Delta e^2} \tag{31}$$

is the minimum splitting of the adiabatic CT surfaces that is achieved at the coordinate

$$X_{min} = \Delta e\Delta F_s^I + \Delta e^2\Delta E \tag{32}$$

For a realistic analysis of optical band shapes, one needs to include the effect of skeletal solute vibrations.[2,6,13] One effective vibrational mode with the frequency ν_v and the vibrational reorganization energy λ_v is commonly considered.[14] For uncoupled intramolecular and solvent nuclear modes, the Franck−Condon envelope is built on the overlap integrals of the harmonic vibronic wave function. Equation 29 then generalizes to[13c,d,f]

$$J_{abs,em}(\nu) = \frac{h}{Q_{\mp}}\sum_{m=-\infty}^{\infty}\sum_{k=1,2} \exp[-S(2\bar{n}_B + 1) + \beta h\nu_v m/2 - \beta F_{\mp}(X_{km}^*)]$$
$$|\Delta E'(X_{km}^*)|^{-1} I_m(2S\sqrt{\bar{n}_B(\bar{n}_B + 1)}) \tag{33}$$

Here, $I_m(x)$ is the modified Bessel function, $S = \lambda_v/h\nu_v$, $\bar{n}_B = [\exp(\beta h\nu_v) - 1]^{-1}$ is the boson occupation number, X_{km}^* is given by eq 30 in which $h\nu$ is replaced by $h\nu \mp mh\nu_v$, and

$$\Delta E'(X_{km}^*) = \frac{dE(X)}{dX}\Big|_{X = X_{km}^*} \tag{34}$$

The limiting vibronic frequency is thus shifted for each vibronic mode to the value

$$h\nu_{min}^{(m)} = \pm mh\nu_v + \Delta E_{min} \tag{35}$$

Equation 33 holds for an arbitrary effective frequency of the skeletal solute vibrations. When the vibrational mode is in the quantum domain satisfying the condition $\beta h\nu_v \gg 2\ln(2S)$, eq 33 simplifies to the relation similar to that commonly applied in the band shape analysis[14]

$$J_{abs,em}(\nu) = \frac{h}{Q_{\mp}}\sum_{m=0}^{\infty}\sum_{k=1,2}\frac{e^{-S}S^m}{m!}|\Delta E'(X_{km}^*)|^{-1}\exp[-\beta F_{\mp}(X_{km}^*)] \tag{36}$$

3. Optical Shifts and Widths

Equation 30 is very important for understanding the optical band shapes. It indicates that the incident light can produce electronic transitions between the two CT surfaces only if its energy $h\nu$ is higher than the low-energy boundary

$$h\nu_{min} = E_{min} \tag{37}$$

The limiting frequency ν_{min} is equal to zero at $\Delta e = 1$ so that optical transitions with arbitrary photon energy are allowed for electronically localized complexes (Robin−Day class II[5]). The limiting frequency increases with increasing delocalization confining the range of energies accessible to optical transitions. Intensities of absorption and emission transitions are always zero at $\nu < \nu_{min}$. This has a profound effect on optical band shapes. Whenever an optical line approaches the boundary ν_{min}, it attains a nonlinear squeezing from its red wing. The line gets skewed and the effective spectral width decreases. For positively solvatochromic dyes with the major multipole higher in the excited state than in the ground state, emission lines are shifted stronger to the red side of the spectrum than the absorption lines. Therefore, the emission lines are closer to the low-energy

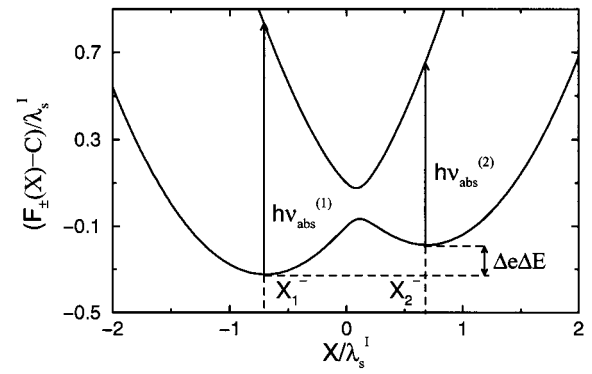

Figure 2. CT adiabatic free energy surfaces in the normal CT region. $h\nu_{abs}^{(1)}$ and $h\nu_{abs}^{(2)}$ indicate the two adiabatically split absorption transitions; $\Delta e = 0.7$, $\Delta F_s^I = 0$, $\Delta E/\lambda_s^I = 0.2$.

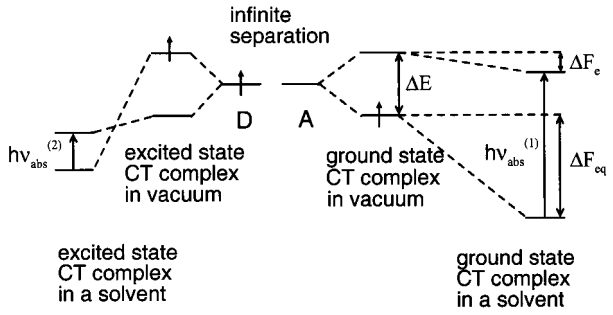

Figure 3. A diagram illustrating the origin of two absorption transitions in delocalized CT complexes. The donor and acceptor energies, equal at infinite separation, split to the energy gap ΔE with formation of the donor−acceptor complex in the gas phase. In a condensed medium, the initial state gains the equilibrium free energy of solvation (ΔF_{eq}). The final state of the Franck−Condon transition is solvated by the fast electronic subsystem only (ΔF_e).

boundary ν_{min} and get narrower than the absorption lines (see section 3.2 below). The opposite trend holds for negatively solvatochromic dyes with higher major multipoles in their ground states.

3.1. Normal CT Region. Only absorption transitions can be observed in the normal CT region (Figure 2). Two vertical transitions exist: one from the ground CT state and the other from the adiabatically split, excited state. The origin of two CT transitions for self-exchange transitions ($\Delta F_s^I = 0$) is illustrated in Figure 3. The donor and acceptor have equal electronic energies at the infinite separation. Their coupling in a CT donor−acceptor complex results in a donor−acceptor electronic overlap breaking the energy symmetry and resulting in the vacuum splitting ΔE ($\Delta E = 2|H_{ab}|$, $|H_{ab}|$ is the diabatic ET matrix element). When transferred to a condensed phase, the initial state of each adiabatically split electronic term is solvated by the equilibrium (electronic+nuclear) polarization of the solvent (ΔF_{eq} in Figure 3), whereas the final state of the vertical Franck−Condon transition is solvated by the electronic solvent polarization only (ΔF_e in Figure 3). The difference, together with the nuclear intramolecular reorganization, brings about the reorganization component in the spectral transition energy which for $(\Delta E + \Delta F_s^I)/\lambda_s^I < 1$ becomes

$$h\nu_{abs}^{(1)} = \lambda_v + \lambda_s^I + \Delta F_s^I + \Delta e\Delta E \tag{38}$$

and

$$h\nu_{abs}^{(2)} = \lambda_v + \lambda_s^I - \Delta F_s^I - \Delta e\Delta E \tag{39}$$

The difference between the absorption frequencies is due to the equilibrium free energy gap between the lower surface minima

$$\Delta F_0 = \Delta e\Delta E + \Delta F_s^I = \frac{h}{2}[\nu_{abs}^{(1)} - \nu_{abs}^{(2)}] \tag{40}$$

The general solution for the absorption band shape composed of two absorption transitions weighted according to their relative thermal populations and the intramolecular vibrational excitations of the solute is given by eq 33 or eq 36. From eqs 14, 15, 26, and 36, one then obtains for the extinction coefficient

$$\bar{\nu}\epsilon(\nu) = 36.8\frac{f(n_D)^2}{(1+\xi)n_D}\frac{(\Delta m_{12}\Delta E)^2}{\sqrt{T\lambda_s^I}}$$

$$\sum_{m=0}^{\infty}\sum_{k=1,2}\frac{e^{-S}S^m}{m!}|\Delta E'(X_{km}^*)|^{-1}\exp[-\beta F_-(X_{km}^*) + \beta F_-(X_1^-)] \tag{41}$$

with

$$X_{km}^* = X_{min} \mp \Delta e\sqrt{(\bar{\nu} - m\bar{\nu}_v)^2 - \Delta E_{min}^2} \tag{42}$$

where "−" and "+" refer to $k = 1$ and $k = 2$, respectively. In eqs 41 and 42, all the energy parameters (X, k_BT, $F_-(X)$, λ_s^I, and ΔE) are in cm^{-1}, m_{12} in D, and T is in K. The parameter ξ in eq 41 is the ratio of populations of in the second (X_2^-) and first (X_1^-) minima of the lower adiabatic surface, $\xi = \exp[-\beta\Delta F_0]$.

If the intramolecular reorganization energy is small, the line profile is given by two superimposed Gaussian lines, shifted relative to each other by $2(\Delta e\Delta E + \Delta F_s^I)$

$$J_{abs}(\upsilon) = h(1+\xi)^{-1}[G_1(\nu) + \xi G_2(\nu)] \tag{43}$$

with

$$G_i(\nu) = (4\pi k_B T\lambda_s^I)^{-1/2}\exp\left[-\beta\frac{(h\nu - h\nu_{abs}^{(i)})^2}{4\lambda_s^I}\right] \tag{44}$$

The width of each absorption band in eq 43 is determined by the invariant reorganization energy λ_s^I. This occurs despite the fact that the curvatures of two wells of the lower CT surface (Figure 2) scale quadratically with Δe.[12] The elimination of the scaling with the delocalization parameter in the observable bandwidth is a result of the cancellation of the quadratic dependence of the curvatures of $F_-(X)$ at the minima $X_{1,2}^-$ with the approximately inverse scaling of the energy gap $\Delta E(X) \simeq |X|/\Delta e$ in the regions close to the well minima. This indicates that the invariant reorganization energy λ_s^I (and not λ_s^d) is the true observable parameter reflected by the spectral width of the solvent-induced component in the absorption vibronic envelope.

Equation 41 extends the conventional band shape analysis of ET in localized systems[13,14,23] to delocalized CT transitions. It can thus be employed to extract CT activation parameters from absorption CT spectra. Application of eq 41 to self-exchange CT systems studied by Nelsen's group[24] is shown in Figure 4. The fitting procedure employs the simulated annealing technique[25] in the space of four activation parameters: λ_s^I, λ_v, ν_v, and ΔE. The magnitude of the delocalization parameter Δe is self-consistently calculated by integrating the absorption profile (eq 79 in ref 12) at each simulation step in the parameters coordinates. The fitting parameters are listed in Table 1. Also

TABLE 1: Parameters of CT Self-exchange Transitions Extracted from the Fit of Experimental Spectra in Acetonitrile[24] to Equation 41 (Figure 4): All Energy Parameters in 10^3 cm^{-1}

compound[a]	r_{12}, Å[b]	r_{ab}, Å[c]	$r_{N,N}$, Å[d]	Δe	λ_s^I	λ_v	$h\nu_v$	$\Delta E/2$	$\lvert H_{ab}^{GMH}\rvert$[e]
2+	4.60	6.63	6.99	0.57	8.89	3.14	1.38	1.66	1.34
3+	5.25	7.37	7.36	0.58	11.24	2.54	1.25	1.13	0.92

[a] Donor−acceptor CT complexes according to ref 24: 1,4-Bis(2-*tert*-butyl-2,3-diazabicyclo[2.2.2]oct-3-yl)benzene-1,4-diyl (**2**) and its 2,5-dimethyl derivative (**3**). [b] ESR measurements.[24] [c] According to eq 45. [d] Crystallographic *N,N*-distance between the t-Bu nitrogens of the hydrazine units gives an estimate of the geometric separation of the donor and acceptor. [e] GMH ET matrix element calculated as $|H_{ab}^{GMH}| = \Delta e|H_{ET}|$ from eq 81 in ref 12.

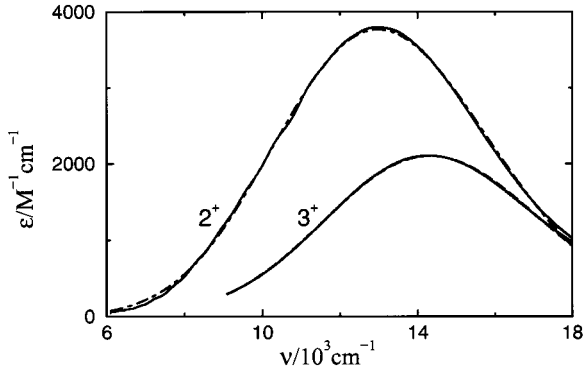

Figure 4. Fits of experimental spectra in acetonitrile[24] (solid lines) to eq 41 (dash−dotted lines, almost indistinguishable from the experimental spectra on the graph scale). The labeling of the donor−acceptor complexes is according to ref 24. The fitting parameters are listed in Table 1.

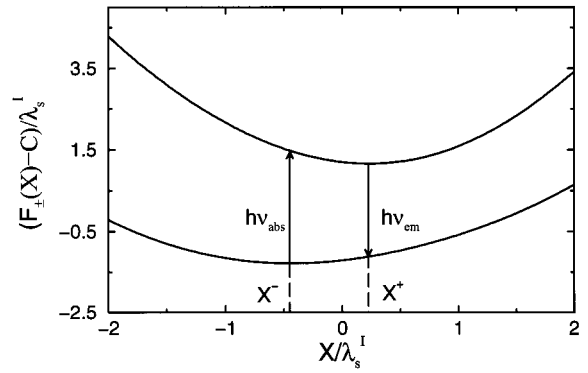

Figure 5. CT adiabatic free energy surfaces in the CT inverted region; $\Delta e = 0.7$, $\Delta F_s^I/\lambda_s^I = -1.0$, $\Delta E/\lambda_s^I = 3.0$. X^- and X^+ indicate the minima of the lower and upper adiabatic surfaces, respectively.

included are estimates of the diabatic ET distance r_{ab} obtained from r_{12} and Δe according to the relation[12]

$$\Delta e = \left[1 + \frac{r_{ab}^2}{r_{12}^2}\right]^{-1/2} \tag{45}$$

valid for self-exchange transitions. The diabatic distances appear to be close to geometric distances between the centers of hydrazine units in the donor−acceptor complexes (cf. columns 3 and 4 in Table 1). Also shown are the GMH ET matrix elements[26] obtained through integrated absorption intensity (eq 81 in ref 12). As is seen, the GMH ET matrix elements are lower than the diabatic matrix element defined for self-exchange transitions as $|H_{ab}| = \Delta E/2$. This result is expected as the GMH basis generates the smallest matrix element among various choices of diabatic basis sets.[26]

3.2. Inverted CT Region. Large adiabatic free energy gaps ΔF_0^{ad} produce the inverted CT region (Figure 5) where both the absorption and emission transitions can in principle be observed.

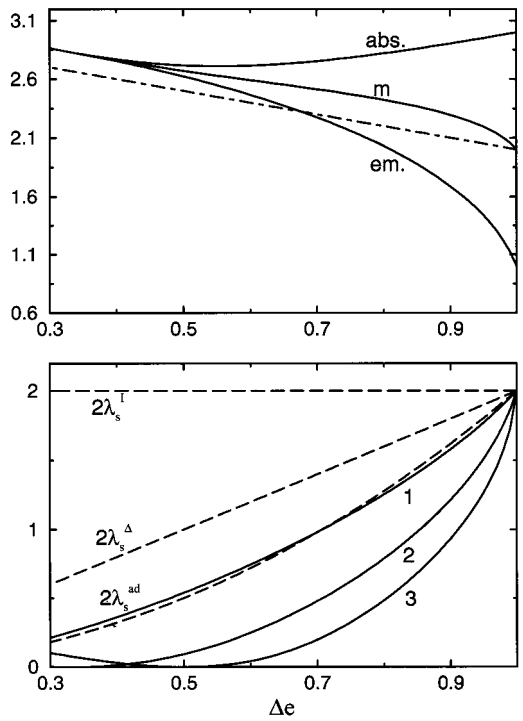

Figure 6. Upper panel: the dependence of the absorption (abs.) and emission (em.) band maxima and their mean (m) on the delocalization parameter. The dash−dotted line indicates the approximation $h\nu_m = \Delta E + \Delta e\Delta F_s^I$; $\Delta F_s^I/\lambda_s^I = -1$ Lower part: the Stokes shift vs the delocalization parameter for $\Delta F_s^I/\lambda_s^I$ equal to 0 (1), −1.0 (2), and −1.5 (3). The dashed lines refer to twice the invariant reorganization energy ($2\lambda_s^I$), the separation of the lower and upper minima ($2\lambda_s^\Delta$), and twice the adiabatic solvent reorganization energy ($2\lambda_s^{ad} = 2\Delta e^2\lambda_s^I$). All energies are dimensionless in units of λ_s^I, $\Delta E/\lambda_s^I = 3.0$.

The positions of the corresponding band maxima are given by the vertical energy gap $\Delta E(X)$ evaluated at the positions of the minima of the lower surface, X^-, and the upper surface, X^+ (Figure 5). The solvent-induced Stokes shift (eq 1) and the mean transition energy (eq 5) are then given by the following relations

$$h\Delta\nu_s^{st} = 2\lambda_s^I - \Delta e^2\lambda_s^I(\Delta E + \Delta F_s^I/\Delta e)\left(\frac{1}{X^+} + \frac{1}{X^-}\right) \tag{46}$$

$$h\nu_m = \frac{\Delta e^2\lambda_s^I}{2}(\Delta E + \Delta F_s^I/\Delta e)\left(\frac{1}{X^+} - \frac{1}{X^-}\right) \tag{47}$$

where the positions of the minima are obtained by solving the equation

$$X^\pm(\Delta E(X^\pm) \pm \lambda_s^I) = \pm\Delta e^2\lambda_s^I(\Delta E + \Delta F_s^I/\Delta e) \tag{48}$$

Absorption and emission energies vary substantially with the delocalization parameter Δe (Figure 6, upper part). Their mean

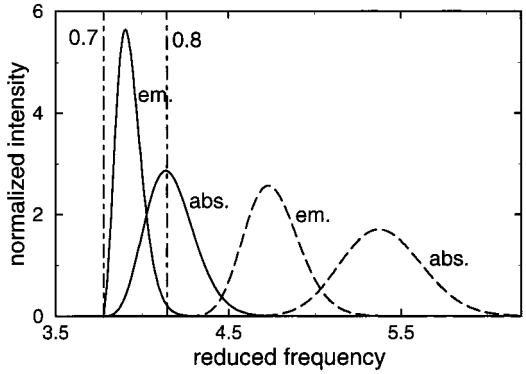

Figure 7. The normalized absorption (abs) and emission (em) intensities at $\Delta e = 0.7$ (solid lines) and $\Delta e = 0.8$ (long-dashed lines) vs the reduced frequency $h\nu/\lambda_s^I$. The dash−dotted lines indicate the lower boundary for the energy of the incident light ν_{min} (eq 31). The calculations are performed for the model chromophore (see text) in the dielectric with $\epsilon_s = 50$.

is a more gently sloping curve that can roughly be approximated as

$$h\nu_m \simeq \Delta E + \Delta e \Delta F_s^I \tag{49}$$

(dash−dotted lines in the upper part in Figure 6). The Stokes shift, on the contrary, is a steeply decaying function of Δe (Figure 6, lower part), especially at Δe close to unity. It deviates strongly from twice the invariant reorganization energy, does not follow the linear scaling of the difference in the minima positions

$$2\lambda_s^\Delta = |X^+ - X^-| \tag{50}$$

and follows the adiabatic reorganization energy λ_s^{ad} only for $\Delta F_s^I = 0$ (Figure 6, lower part, line 1). The latter situation is, however, unrealistic for transitions in the inverted ET region with usually a substantial solvation component of the equilibrium free energy gap. The dependence of the Stokes shift on Δe becomes steeper with more negative equilibrium solvation energies (Figure 6, lower part, lines 2 and 3). This means that for $\Delta e < 1$ the Stokes shift does not measure the reorganization energy alone and the mean of the transition energies provides only an approximate measure of the equilibrium energy gap. These two observables should be considered as input parameters to the nonlinear eqs 47 and 46 that are solved in respect to λ_s^I and ΔF_s^I. The solution is, of course, possible only if the vacuum splitting and the delocalization parameter are both known from an independent source.

Electron delocalization also affects substantially the band shapes of the absorption and emission lines. Two basic features of optical spectra of positively solvatochromic dyes with $\Delta e < 1$ are illustrated in Figure 7 (the calculations are performed according to eq 36): (i) the emission width is increasingly smaller than the absorption width with decreasing Δe and (ii) both absorption and emission lines are asymmetric with higher intensities of their blue wings. As mentioned above, these effects are caused by the proximity of the lower boundary ν_{min} of the energies accessible to optical transitions.

To model the evolution of absorption and emission band shapes with solvent polarity we consider a model spherical chromophore of the radius $R_0 = 4$ Å immersed in the dielectric continuum. The adiabatic dipole moments of the chromophore are $m_{01} = 5$ D and $m_{02} = 15$ D. The high-frequency dielectric constant of the solvent is held at $\epsilon_\infty = 2.0$ and the static dielectric constant ϵ_s is varied in the range 10−50. In this model, the adiabatic solvent reorganization energy and the solvation part of the equilibrium free energy gap are

$$\lambda_s^{ad} = \frac{\Delta m_{12}^2}{R_0^3}\left[\frac{\epsilon_s - 1}{2\epsilon_s + 1} - \frac{\epsilon_\infty - 1}{2\epsilon_\infty + 1}\right] \tag{51}$$

and

$$\Delta F_s^{ad} = -\frac{(m_2^2 - m_1^2)}{R_0^3}\frac{\epsilon_s - 1}{2\epsilon_s + 1} \tag{52}$$

The invariant quantities are then obtained by applying the scaling laws[12]

$$\lambda_s^{ad} = (\Delta e)^2 \lambda_s^I \tag{53}$$

and

$$\Delta F_s^{ad} = \Delta e \Delta F_s^I \tag{54}$$

The results of calculations of the transition energies and spectral widths are listed in Table 2.

TABLE 2: Spectral Parameters (10^3 cm^{-1}) of the Model Chromophore (See Text) with $\Delta E = 24.2 \times 10^3$ cm^{-1}

ϵ_s	λ_s^I	λ_s^{ad}	λ_s^{st} [a]	$h\Delta\langle\nu\rangle^{st}/2$ [b]	ΔF_0 [c]	$h\nu_m$	λ_{abs}^w [d]	λ_{em}^w [d]	λ_m^w [e]
				$\Delta e = 0.7$					
10	3.67	2.08	0.58	0.58	14.56	18.82	0.91	0.34	0.63
20	4.23	2.07	0.56	0.57	13.78	18.55	0.97	0.29	0.63
30	4.43	2.17	0.55	0.56	13.52	18.46	0.98	0.27	0.63
40	4.51	2.21	0.54	0.55	13.37	18.40	0.98	0.26	0.62
50	4.56	2.23	0.53	0.55	13.30	18.39	0.99	0.25	0.62
				$\Delta e = 0.8$					
10	2.81	1.80	1.03	0.90	15.75	17.76	1.34	0.74	1.04
20	3.24	2.07	1.10	1.09	15.08	17.91	1.51	0.73	1.12
30	3.39	2.17	1.12	1.11	14.87	17.80	1.58	0.72	1.15
40	3.45	2.21	1.12	1.11	14.73	17.72	1.60	0.72	1.16
50	3.51	2.25	1.12	1.12	14.66	17.70	1.61	0.71	1.16

[a] Difference in the energies of the absorption and emission maxima. [b] Obtained as a difference of the first spectral moments, eq 55. [c] The gap between the free energy minima of the upper and lower surfaces. [d] From half-intensity width according to eq 56. [e] $\lambda_m^w = (\lambda_{abs}^w + \lambda_{em}^w)/2$.

Table 2 reveals several features of optical transitions in delocalized systems. Columns 4 and 5 list the reorganization energies λ_s^{st} obtained from maxima energies (eq 1) and the first spectral moments

$$\langle\nu\rangle_{abs,em} = \int_{-\infty}^{\infty} \nu J_{abs,em}(\nu) d\nu \tag{55}$$

Both Stokes shifts are considerably smaller than the invariant, $\lambda_s^I \simeq \lambda_s^d$, or adiabatic reorganization energies, in contrast to eq 3. The dependence of the Stokes shift on solvent polarity is much weaker than that of the reorganization energy. Also, the equality $\lambda_s^{st} = \lambda_{abs,em}^w$ valid for the linear response with $\Delta e = 1$ does not hold. The mean of the squared absorption and emission widths (column 10) correlates better with the Stokes shift.[27] The Stokes shift increases with solvent polarity at $\Delta e = 0.8$, in accord with traditional theories. At a higher electronic delocalization, $\Delta e = 0.7$, on the other hand, the inverted solvent dependence develops: the reorganization energy and the Stokes shift have the opposite dependence on solvent polarity. This is the result of the proximity of the emission line to the band

TABLE 3: Spectral Parameters (all energies are in 10^3 cm^{-1}) of the Individual Vibronic Excitations Participating in Absorption and Emission Band Shapes (Calculations Are Performed for the Model Chromophore with $\lambda_s^I = 3.4 \times 10^3$ cm^{-1}, $\lambda_v = 3.23 \times 10^3$ cm^{-1}, $h\nu_v = 1500$ cm^{-1}, $\Delta F_s^I = -9.33 \times 10^3$ cm^{-1}, $\Delta e = 0.8$, and $\Delta E = 24.2 \times 10^3$ cm^{-1})

m^a	$h\nu_{abs}{}^b$	$\beta\sigma^2_{abs}{}^c$	$h\nu_{em}{}^d$	$\beta\sigma^2_{em}{}^c$	$h\Delta\nu_s^{st}$	$h\Delta\langle\nu\rangle^{st}$	$h\nu_m$	$I_m(\nu_{abs})^e$	$I_m(\nu_{em})^e$
0	18.92	3.13	16.69	1.45	2.23	2.21	17.81	0.19	0.29
1	20.42	3.15	15.19	1.45	5.23	5.21	17.80	0.42	0.62
2	21.92	3.15	13.69	1.45	8.24	8.21	17.80	0.45	0.66
3	23.42	3.13	12.19	1.45	11.23	11.21	17.80	0.32	0.47
4	24.92	3.13	10.69	1.47	14.23	14.21	17.80	0.17	0.26
5	26.42	3.13	9.19	1.45	17.23	17.21	17.81	0.07	0.11
$\sum_m$	21.66	25.08	13.65	16.86	8.01	8.65	17.65	0.59	0.69

[a] Index of the vibronic band participating in the optical line $\sum_m$ denotes the total spectrum obtained by the superposition of the individual vibronic excitations, as in eq 36. [b] Energy of the individual vibronic absorption line and of the total absorption spectrum. [c] Calculated from the half-intensity width according to eq 56. [d] Energy of the individual emission vibronic line and the total emission spectrum. [e] Intensity at the maximum, the areas under the total absorption and emission lines are normalized to unity.

boundary ν_{min}. With increasing solvent polarity, the absorption line still shifts to the red whereas the emission line almost does not change its position (Figure 7). As a result, the Stokes shift decreases with increasing the reorganization energy λ_s^I.

The absorption and emission widths in Table 2 were obtained from the halt-intensity spectral widths according to the relation

$$\sigma_{abs,em} = \frac{\sigma(^1/_2)_{abs,em}}{(8\ln(2))^{1/2}} \qquad (56)$$

For a Gaussian line, eq 56 produces the second spectral cumulant

$$\langle(\delta\nu)^2\rangle_{abs,em} = \int_{-\infty}^{\infty}(\nu - \nu_{abs,em})^2 J_{abs,em}(\nu)d\nu \qquad (57)$$

The direct use of the second spectral cumulant instead of the half-intensity width gives the results very close to those listed in Table 2.

The emission lines are narrower than the absorption lines for all polarities considered, which is characteristic of the positively solvatochromic dye used in the calculations. For $\Delta e = 0.8$, the absorption width is a rising function of λ_s^{st} whereas the emission width decays with λ_s^{st}. This type of behavior has indeed been observed for the C153 optical dye[28a] (see Figure 8 in ref 28b). C153 possesses a large transition dipole[17b] and a substantial delocalization is thus expected. For $\Delta e = 0.7$, due to the inverted solvent dependence of the Stokes shift, the emission width increases with λ_s^{st} whereas the absorption width decreases with λ_s^{st}. This rich pattern of various types of relations between the optical observables differs qualitatively from the simple relation in eq 4 valid only for $\Delta e = 1$.

Intramolecular vibronic excitations produce manifolds of absorption and emission lines. Their superposition forms the absorption and emission vibronic envelopes (eq 36, Figure 8). The spectroscopic parameters of several most intense individual lines, each corresponding to m quanta of vibrational excitation of the solute, are listed in Table 3. As is seen, all lines from the absorption or emission vibronic envelopes have the same widths and are only shifted relative to each other by ν_v. The lower energy boundary $\nu_{min}^{(m)}$ (eq 35) exists for each vibronic excitation. For the absorption envelope, $\nu_{min}^{(m)}$ shifts to the blue with m thus enhancing the relative weight of the blue side of the spectrum. Oppositely, for emission lines, $\nu_{min}^{(m)}$ decreases with m allowing lower frequency vibronic transitions. The familiar mirror-symmetry[17a] profiles of absorption and emission bands then develop. Still, every solvent-broadened component of the emission envelope is considerably narrower than the corresponding absorption line and the total emission width is much smaller than the absorption width (Table 3). Analogously to the individual vibronic transitions, the emission width of the whole band decays with solvent polarity and the absorption width increases with solvent polarity.

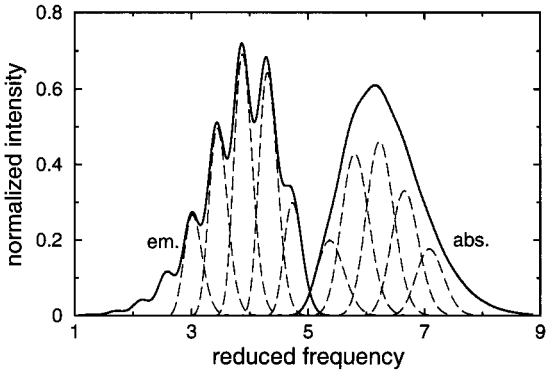

Figure 8. Absorption (abs.) and emission (em.) vibronic envelopes vs $h\nu/\lambda_s^I$. The dashed lines indicate the first five vibrational excitations with $m = 0 - 4$ in eq 36. The parameters of the solute and the solvent are the same as those in Table 3.

A practically important problem is the development of algorithms yielding parameters characteristic of the 0−0 solvent-broadened vibronic transition from the parameters of the whole vibronic envelope. Such a procedure is often referred to as the band shape analysis.[14] From this perspective, eqs 3 and 5 are often used as a source of the reorganization energy and the equilibrium free energy gap of ET. Table 3 indicates that the mean of the absorption and emission lines is indeed a robust parameter characterizing solely the solvent effect. In contrast, the Stokes shift is strongly affected by the vibrational excitations and is not a very dependable source of the solvent reorganization energy. For instance, as is seen from Table 3, half the Stokes shift of the 0−0 transition ($m = 0$) $\lambda_s^{st} = 1115$ cm^{-1} is considerably smaller than the adiabatic reorganization energy $\lambda_s^{ad} = 2176$ cm^{-1}. Also, for delocalized systems, the extraction of the solvent-induced Stokes shift by subtracting its vibrational component according to eq 3 is applicable only in respect to the first spectral moments $\langle\nu\rangle_{abs,em}$. As is illustrated in Figure 9, the difference between $\Delta\langle\nu\rangle^{st}$ and $\Delta\nu^{st}$ increases with delocalization. The gap between the two values is not a monotonic function of vibrational reorganization and the two parameters may be close to each other or widely different depending on the magnitude of $\Delta\nu_v^{st}$. The difference of the first moments $\Delta\langle\nu\rangle^{st}$, however, follows eq 1 for all values of the delocalization parameter.

4. Discussion

Equations 3−5 lay the foundation for connecting optical and thermal parameters in localized ET systems. They, however,

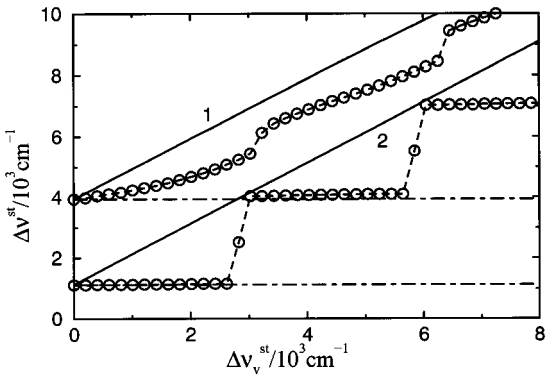

Figure 9. Stokes shift vs the magnitude of its vibrational component for $\Delta e = 0.9$ (1) and $\Delta e = 0.7$ (2). The solid lines indicate $h\Delta\langle\nu\rangle^{st} = h(\langle\nu\rangle_{abs} - \langle\nu\rangle_{em})$, the circles show $h\Delta\nu^{st} = h(\nu_{abs} - \nu_{em})$. The dash−dotted lines correspond to $h\Delta\nu_s^{st}$. The other solute parameters are as in Table 3.

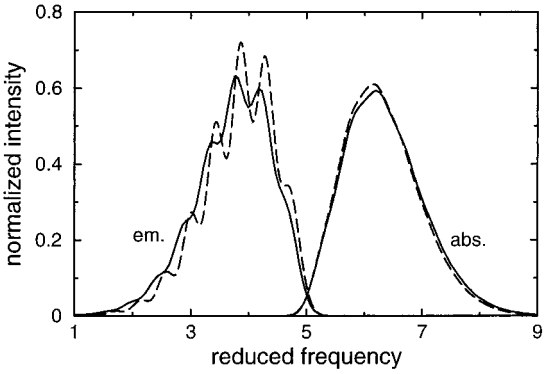

Figure 10. The same vibronic profiles as in Figure 8 (dashed lines) are compared to the band shapes calculated in the Drude oscillator model (solid lines, ref 11) with the solute polarizability of the two-state solute (eq 59). Since there is no direct connection between the diabatic and adiabatic vacuum gaps, the Drude spectra are shifted by a constant energy to ensure coinciding maxima of the 0−0 vibronic transitions of the two absorption vibronic envelopes.

do not hold in delocalized complexes with $\Delta e < 1$. Two manifestations of this come about. First, the solute-induced Stokes shift is less than twice the adiabatic reorganization energy (Figure 6)

$$\lambda_s^{st} \le \lambda_s^{ad} \le \lambda_s^{d} \tag{58}$$

The parameter λ_s^{st} is in fact a complex function of λ_s^{ad}, ΔF_s^{ad}, and Δe (eqs 47 and 46). It does not characterize the reorganization energy alone as well as the mean frequency (eq 5) does not give the equilibrium energy gap. Second, the vibrational component of the vibronic envelope affects in a complex way the positions of the spectral maxima. The subtraction of the vibrational component of the observed Stokes shift in order to extract its solvent-induced component works only if the first spectral moments are used as the measure of the shift (Figure 9). The use of maxima positions instead of the first spectral moments leads to errors increasing with delocalization.

Equation 4 relating spectral widths to the reorganization energy also does not hold at $\Delta e < 1$. The adiabatic free energies increasingly split with decreasing Δe. The minimum photon energy $h\nu_{min}$ sufficient to cover the gap rises with decreasing Δe. The boundary of the band of the energy gap fluctuations of the solute then blue-shifts. As this boundary approaches the position of an emission line ($\Delta m_{12} > 0$), the emission line narrows compared to the absorption line (Table 2, Figure 7). Another manifestation of this effect is the development of the inverted solvent dependence of the Stokes shift: at Δe close to unity the Stokes shift increases with solvent polarity whereas for smaller Δe the Stokes shift starts to decrease with solvent polarity (Table 2).

The two-state approximation and its multistate extensions are often considered to model the electronic polarizability of the solute.[10a−c] The Drude oscillator model[29] is another theoretical tool for this purpose. We have recently considered electronic transitions in a polarizable solute within the framework of the Drude model[11] and a comparison of the two approaches seems pertinent here. A connection between the two-state and Drude models can be drawn by noticing that a two-state dipolar solute with the transition moment m_{12} generates the polarizability

$$\alpha_{0i} = \pm\frac{2m_{12}^2}{\Delta E} \tag{59}$$

that is positive in the ground state and negative in the exited state. In Figure 10, the vibronic absorption and emission envelopes obtained in the present two-state description are compared to the same spectra following from the Drude model considered in ref 11 with the ground and excited-state polarizabilities given by eq 59. Though not equivalent, the spectra are nevertheless very close indicating that the two models produce similar optical band shapes.

Of course, the two-state truncation is very unrealistic in predicting the solute polarizability that commonly increases with excitation.[16] The Drude oscillator model is thus preferable for describing the polarizability effects. The Drude model gives, however, only diabatic free energy surfaces. It does not, therefore, include the modification of the activation barrier of thermal CT by electronic delocalization. A two-state description (with a possible generalization to many states) in terms of adiabatic CT surfaces is a better choice for describing the delocalization effects. However, a proper account of polarizability effects is hard to achieve by a multistate extension of this approach as many states are needed to get the polarizability right.[30] In view of the complications characteristic of each of the models, a hybrid description can be sought to include both the delocalization and polarizability effects. The two states involved in electronic transitions can be treated explicitly in terms of the two-state model with the Drude model used to describe the polarizability arising from the virtual transitions to all other electronic states. A generalization of the current theory along these lines is presently underway.

5. Conclusions

Classical theories of the solvent effect on optical band shapes[1] consider interaction of the charge distribution of the solute with the solvent as the source of the solvent-induced band-shift and inhomogeneous broadening. The present development shows that solvation of the off-diagonal matrix element of the solute field, represented here by the transition dipole, considerably modifies optical band shapes. Therefore, in many practical situations, optical shifts and widths of intense optical lines should depend not only on the initial and final dipoles of the chromophore, but, to a large extent, on the transition dipole. The band shape analysis of optical lines is extended to include this feature. It turns out that the linear response relations widely used to connect optical observables to CT activation parameters (eqs 3−5) break down for electronically delocalized systems generating essentially nonlinear features of the solvent effect on optical lines. The CT parameters are thus solutions of

nonlinear equations involving the absorption and emission transition energies, the vacuum energy gap, and the delocalization parameter. The optical spectra attain the low-energy boundary caused by the adiabatic splitting of the free energy surfaces. This boundary blue-shifts with increasing electronic delocalization resulting in different widths for absorption and emission as well as asymmetries of the optical bands.

Acknowledgment. We thank Prof. S. F. Nelsen for useful comments and for spectral data from ref 24. This research was supported by the Basic Energy Sciences Branch of the Department of Energy through Grant DE-FG03-99ER14963.

References and Notes

(1) Liptay, W. In *Modern Quantum Chemistry*; Sinano glu, Ed.; Acedemic Press: New York, 1965. (b) Amos, A. T.; Burrows, B. L. In *Advances in Quantum Chemistry*; Löwdin, P.-O., Ed.; Academic Press: New York, 1973; Part II.

(2) Lax, M. *J. Chem. Phys.* **1952**, *20*, 1752.

(3) Stoneham, A. M. *Rev. Mod. Phys.* **1969**, *41*, 82.

(4) (a) Marcus, R. A. *J. Chem. Phys.* **1965**, *43*, 679. (b) Hush, N. S. *Prog. Inorg. Chem.* **1967**, *8*, 391. (c) Creutz, C. *Prog. Inorg. Chem.* **1983**, *30*, 1.

(5) (a) Robin, M. B.; Day, P. In *Advances in Inorganic Chemisttry and Radiochemistry*; Emeléus, H. J., Sharpe, A. G., Eds.; Academic Press: New York, 1967; Vol. 10. (b) Crutchley, R. J. In *Advances in Inorganic Chemistry, V. 41*; Sykes, A. G., Eds.; Academic Press: San Diego, 1994.

(6) Marcus, R. A. *J. Phys. Chem.* **1989**, *93*, 3078.

(7) (a) Chandler, D. *Phys. Rev. E* **1993**, *48*, 2898. (b) Song, X.; Chandler, D.; Marcus, R. A. *J. Phys. Chem.* **1996**, *100*, 11954.

(8) The transition frequencies $\nu_{abs,em}$ are commonly understood either as maxima positions or as the first spectral moments. We will distinguish between these two definitions labeling the energies of the band maxima as $\nu_{abs,em}$ and use $\langle\nu\rangle_{abs,em}$ for the first spectral moments.

(9) (a) Kuharski, R. A.; Bader, J. S.; Chandler, D.; Sprik, M.; Klein, M. L.; Impey, R. W. *J. Chem. Phys.* **1988**, *89*, 3248. (b) King, G.; Warshel, A. *J. Chem. Phys.* **1990**, *93*, 8682. (c) Fonseca, T.; Ladanyi, B. M.; Hynes, J. T. *J. Phys. Chem.* **1992**, *96*, 4085. (d) Ichiye, T. *J. Chem. Phys.* **1996**, *104*, 7561.

(10) (a) Bursulaya, B. D.; Zichi, D. A.; Kim, H. J. *J. Phys. Chem.* **1995**, *99*, 10069. (b) Kim, H. J. *J. Chem. Phys.* **1996**, *105*, 6818. (c) Ando, K. *J. Chem. Phys.* **1997**, *107*, 4585. (d) Schmitt, U. W.; Voth, G. A. *J. Phys. Chem.* **1998**, *102*, 5547.

(11) Matyushov, D. V.; Voth, G. A. *J. Phys. Chem. A* **1999**, *103*, 10981.

(12) Matyushov, D. V.; Voth, G. A. *J. Phys. Chem. A* **2000**, *104*, 6470.

(13) (a) Huang, K.; Rhys, A. *Proc. R. Soc.* **1950**, *204A*, 406. (b) Kubo, R.; Toyozawa, Y. *Prog. Theor. Phys.* **1955**, *13*, 160. (c) Kestner, N. R.; Logan, J.; Jortner, J. *J. Phys. Chem.* **1974**, *78*, 2148. (d) Mahan, G. D. *Many-Particle Physics*; Plenum Press: New York, 1990; Chapter 4.3. (e) Bixon, M.; Jortner, J.; Cortes, J.; Heitele, H.; Michel-Beyerle, M. E. *J. Phys. Chem.* **1994**, *98*, 7289. (f) Bixon, M.; Jortner, J. *Adv. Chem. Phys.* **1999**, *106*, 35.

(14) (a) Walker, G. C.; Åkesson, E.; Johnson, A. E.; Levinger, N. E.; Barbara, P. F. *J. Phys. Chem.* **1992**, *96*, 3728. (b) Cortés, J.; Heitele, H.; Jortner, J. *J. Phys. Chem.* **1994**, *98*, 2527.

(15) Onsager, L. *J. Am. Chem. Soc.* **1936**, *58*, 1486.

(16) (a) Liptay, W. In *Excited States*; Lim, E. C., Ed.; Academic Press: New York, 1974; Vol. 1. (b) Oh, D. H.; Sano, M.; Boxer, S. G. *J. Am. Chem. Soc.* **1991**, *113*, 6880. (c) Vance, F. W.; Williams, R. D.; Hupp, J. T. *Int. Rev. Phys. Chem.* **1998**, *17*, 307.

(17) (a) Birks, J. B. *Photophysics of Aromatic Molecules*; Wiley: London, 1970. (b) Lewis, J. L.; Maroncelli, M. *Chem. Phys. Lett.* **1998**, *282*, 197.

(18) Matyushov, D. V.; Ladanyi, B. M. *J. Phys. Chem. A* **1998**, *102*, 5027.

(19) (a) Gould, I. R.; Noukakis, D.; Gomez-Jahn, L.; Young, R. H.; Goodman, J. L.; Farid, S. *Chem. Phys.* **1993**, *176*, 439. (b) Gould, I. R.; Young, R. H.; Mueller, L. J.; Albrecht, A. C.; Farid, S. *J. Am. Chem. Soc.* **1994**, *116*, 8188.

(20) (a) Murrell, J. N. *J. Am. Chem. Soc.* **1959**, *81*, 5037. (b) Mulliken, R. S.; Person, W. B. *Molecular Complexes*; Wiley: New York, 1969.

(21) (a) Ernsting, N. P.; Asimov, M.; Schäfer, F. P. *Chem. Phys. Lett.* **1982**, *91*, 231. (b) Mühlpfordt, A.; Schanz, R.; Ernsting, N. P.; Farztdinov, V.; Grimme, S. *Phys. Chem. Chem. Phys.* **1999**, *1*, 3209.

(22) Köhler, G.; Rechthalter, K.; Grabner, G.; Luboradski, R.; Suwińska, K.; Rotkiewicz, K. *J. Phys. Chem. A* **1997**, *101*, 8518.

(23) Chen, P.; Meyer, T. J. *Chem. Rev.* **1998**, *98*, 1439.

(24) Nelsen, S. F.; Ismagilov, R. F.; Powell, D. R. *J. Am. Chem. Soc.* **1997**, *119*, 10213.

(25) Press, W. H.; Teukolsky, S. A.; Vetterling, W. T.; Flannery, B. P. *Numerical Recipes in Fortran 77: The Art of Scientific Computing*; Cambridge University Press: Cambridge, 1992; Vol. 1.

(26) (a) Cave, R. J.; Newton, M. D. *Chem. Phys. Lett.* **1996**, *249*, 15. (b) Newton, M. D.; Cave, R. J. In *Molecular Electronics*; Ratner, M. A., Jortner, J., Eds.; IUPAC: London, 1997.

(27) Stephens, M. D.; Saven, J. G.; Skinner, J. L. *J. Chem. Phys.* **1997**, *106*, 2129.

(28) (a) Horng, M. L.; Gardecki, J. A.; Papazyan, A.; Maroncelli, M. *J. Phys. Chem.* **1995**, *99*, 17311. (b) Matyushov, D. V.; Ladanyi, B. M. *J. Chem. Phys.* **1997**, *107*, 1375.

(29) (a) Pratt, L. R. *Mol. Phys.* **1980**, *40*, 347. (b) Thompson, M. J.; Schweizer, K. S.; Chandler, D. *J. Chem. Phys.* **1982**, *76*, 1128. (c) Høye, J. S.; Stell, G. *J. Chem. Phys.* **1980**, *73*, 461. (d) Chen, Y.-C.; Lebowitz, J. L.; Nielaba, P. *J. Chem. Phys.* **1989**, *91*, 340. (d) Cao, J.; Berne, B. J. *J. Chem. Phys.* **1993**, *99*, 2902.

(30) (a) Bursulaya, B. D.; Kim, H. J. *J. Chem. Phys.* **1998**, *108*, 3277. (b) Newton, M. D. Unpublished.